water

MDPI

Article

Displacement Prediction Method for Rainfall-Induced Landslide Using Improved Completely Adaptive Noise Ensemble Empirical Mode Decomposition, Singular Spectrum Analysis, and Long Short-Term Memory on Time Series Data

Ke Yang [1], Yi Wang [2,*] and Gonghao Duan [3]

[1] School of Geography and Information Engineering, China University of Geosciences, Wuhan 430074, China; yangke@cug.edu.cn
[2] Institute of Geophysics and Geomatics, China University of Geosciences, Wuhan 430074, China
[3] School of Computer Science and Engineering, Wuhan Institute of Technology, Wuhan 430205, China; duangh@wit.edu.cn
* Correspondence: wangyi@whu.edu.cn; Tel.: +86-027-67883257

Abstract: Landslide disasters frequently result in significant casualties and property losses, underscoring the critical importance of research on landslide displacement prediction. This paper introduces an approach combining improved empirical mode decomposition (ICEEMDAN) and singular entropy-enhanced singular spectrum analysis (SSA) to predict landslide displacement using a time series short-duration memory network (LSTM). Initially, ICEEMDAN decomposes the landslide displacement time series into trend and periodic terms. SSA is then employed to denoise these components before fitting the trend term with LSTM. Pearson correlation analysis is utilized to identify characteristic factors within the LSTM model, followed by predictions using a multivariate LSTM model. The empirical results from the Baijiabao landslide in the Three Gorges Reservoir area demonstrate that the joint ICEEMDAN-SSA approach, when combined with LSTM modeling, outperforms the separate applications of SSA and ICEEMDAN, as well as other models such as RNN and SVM. Specifically, the ICEEMDAN-SSA-LSTM model achieves an RMSE of 6.472 mm and an MAE of 4.992 mm, which are considerably lower than those of the RNN model (19.945 mm and 15.343 mm, respectively) and the SVM model (16.584 mm and 11.748 mm, respectively). Additionally, the R^2 value for the ICEEMDAN-SSA-LSTM model is 97.5%, significantly higher than the RNN model's 72.3% and the SVM model's 92.8%. By summing the predictions of the trend and periodic terms, the cumulative displacement prediction is obtained, indicating the superior accuracy of the ICEEMDAN-SSA-LSTM model. This model provides a new benchmark for precise landslide displacement prediction and contributes valuable insights to related research.

Keywords: landslide; ICEEMDAN-SSA-LSTM; temporal prediction; displacement decomposition

Citation: Yang, K.; Wang, Y.; Duan, G. Displacement Prediction Method for Rainfall-Induced Landslide Using Improved Completely Adaptive Noise Ensemble Empirical Mode Decomposition, Singular Spectrum Analysis, and Long Short-Term Memory on Time Series Data. *Water* **2024**, *16*, 2111. https://doi.org/10.3390/w16152111

Academic Editor: Francesco De Paola

Received: 26 June 2024
Revised: 21 July 2024
Accepted: 22 July 2024
Published: 26 July 2024

1. Introduction

Landslides are prevalent geological disasters that not only result in significant casualties but also lead to substantial economic losses. There are primarily two approaches for the monitoring and early warning of landslides: one relies on historical data prediction, and the other utilizes theoretical analysis. The choice of method for landslide displacement prediction often depends on the specific circumstances and available technologies. With advancements in UAV remote sensing and 3D laser scanning, it is now possible to monitor landslides extensively, although these methods produce data characterized by high noise levels and large volumes, posing challenges in extracting useful information and developing effective prediction models.

Historical research has explored various predictive models for landslide displacement. For instance, in 2017, Shihabudheen advocated the use of the Extreme Learning Machine

(ELM) to address challenges like gradient descent in landslide prediction [1]. In 2020, Wang Yankun et al. utilized two Least Squares Support Vector Machine (LSSVM) models, enhanced by a differential search algorithm, to forecast future displacement intervals and optimize model parameters [2]. Furthermore, Wu introduced a metabolism-based GM(1,1) model that dynamically updates to improve prediction accuracy over the traditional GM(1,1) model [3]. Most recently, in 2022, Zian Lin et al. combined an exponentially weighted moving average (EWMA) method with a Double-BiLSTM model to predict landslide displacements, demonstrating significant advancements from initial singular model applications to complex multi-model approaches [4].

Current methodologies in landslide displacement prediction fall into three categories: constructing time series models from periodic monitoring data [5], integrating landslide data with time series models like ARIMA and PSO-LSTM [6], and developing enhanced models through innovative techniques [7]. The first two methods effectively handle non-stationary signals but require extensive data for model training and may not capture all characteristics of landslide displacement time series. The third approach, which includes novel decomposition and noise reduction techniques, tends to preserve time series features more effectively, though some data may be lost during the process.

Regarding specific techniques, the ICEEMDAN method is noted for its superior signal decomposition capabilities [8], SSA is recognized for its effective denoising properties [9], and the LSTM model is particularly advantageous for predicting long series data due to its ability to handle such complexities, making it a common choice in time series prediction [10]. Despite their strengths, these methods are not frequently employed in landslide displacement prediction, suggesting an area for further exploration and application in geotechnical forecasting.

This paper introduces a combined approach using ICEEMDAN, SSA, and LSTM to process landslide displacement data, where ICEEMDAN decomposes the data into trend and periodic terms, SSA performs noise reduction, and LSTM models predict these components. This study employs the Baijiabao landslide as a case study to demonstrate the efficacy of the ICEEMDAN-SSA-LSTM model against conventional methods. The results indicate that this model not only effectively removes trend and noise from non-stationary landslide data but also achieves superior prediction accuracy. This integrated model offers a novel perspective for predicting landslide hazards, suggesting a promising direction for future research in this field.

2. Research Flowchart

This paper explores the technical process of landslide prediction from the perspective of displacement decomposition. We introduce the ICEEMDAN-SSA-LSTM model to enhance the accuracy of landslide displacement data prediction. Initially, displacement data are decomposed into trend and periodic terms using ICEEMDAN, SSA, and a combined ICEEMDAN-SSA approach. Subsequently, these decomposed terms are predicted using an LSTM model. The performance of each model is evaluated by comparing their prediction accuracy. To further assess the feasibility of this hybrid model, traditional models such as RNN and SVM are incorporated into the prediction of periodic terms for comparative analysis. The error metrics of the prediction results from each model are thoroughly reviewed. This study uses the Baijiabao landslide as a case study, with Figure 1 illustrating the detailed research process.

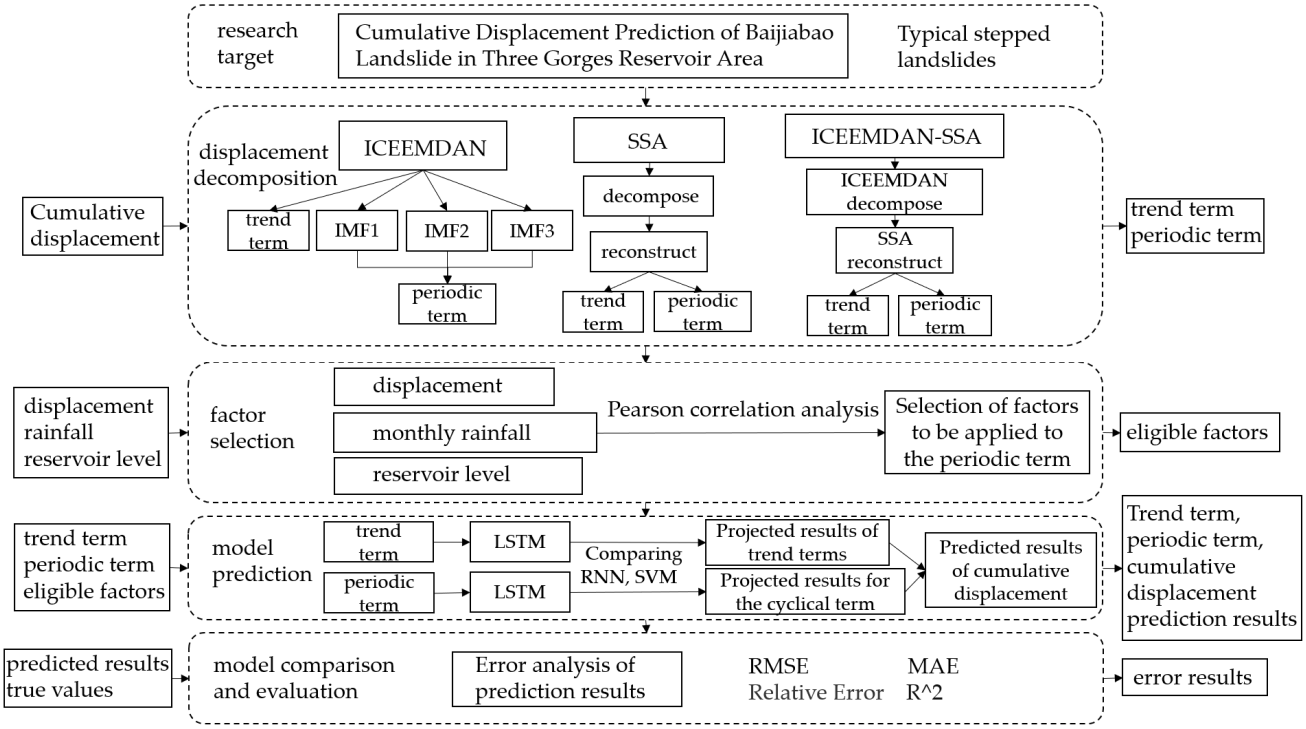

Figure 1. Research flowchart.

3. Materials and Methods

3.1. Geological Situation and Time Series Data of Baijiabao Landslide

The Baijiabao Landslide is situated within the second group of Xiangjiadian Village, Guizhou Town, Zigui County, located in the Three Gorges Reservoir area, approximately 2.5 km from the confluence of the Xiangxi River and the Yangtze River. It lies 41.2 km from the Three Gorges Dam, positioned on the right bank of the Xiangxi River, a northern tributary of the Yangtze River. The geographical coordinates of the landslide are 30°58′59.9″ N, 110°45′33.4″ E. The terrain at the landslide site is complex, featuring a mix of gentle slopes and gullies, leading to varied landforms. The sliding surface of the landslide typically presents an arc shape. The profile and the distribution of monitoring equipment locations are illustrated in Figure 2. The data were derived from field survey data of the landslide site.

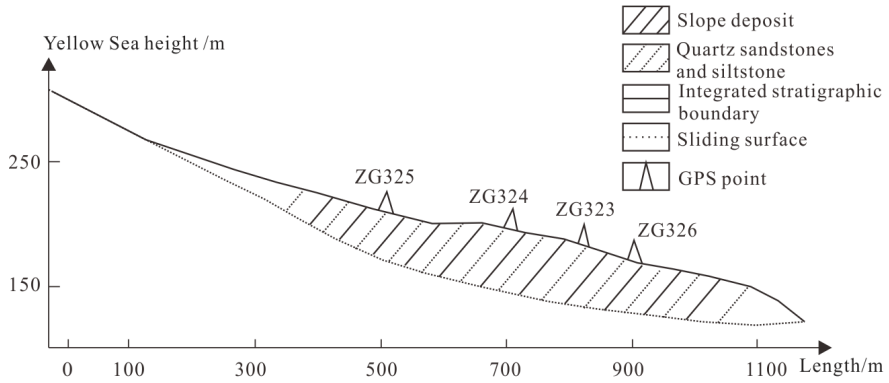

Figure 2. Section view of Baijiabao landslide.

The Baijiabao landslide is situated on the right bank of the Xiangxi River, a tributary of the northern bank of the Yangtze River. Seasonally, the area experiences precipitation predominantly from April to September, characterized by cooler temperatures in winter and rainy, humid, and warmer summers. Structurally, two distinct groups of geological

joints are identified at the landslide site; one group facilitates the collapse of the landslide's trailing edge, while the other bisects the landslide into left and right segments [11].

To safeguard the lives and property of the local villagers, GNSS-based surface displacement monitoring of the Baijiabao landslide commenced in October 2006. This monitoring strategy utilizes multiple GNSS sensors strategically placed across the landslide to record precise displacement data, culminating in comprehensive datasets on the cumulative displacement. Over time, this allows researchers to trace and analyze the progression of deformation within the landslide. For this initiative, four monitoring sites designated as ZG323, ZG324, ZG325, and ZG326 were established. Sites ZG324 and ZG325 are located in the principal area of landslide activity, while ZG323 and ZG326 are positioned in the middle and lower sections, near the Zixing. The instrumentation employed delivers exceptionally high measurement accuracy [12].

From November 2006 to December 2011, data from four displacement sensors—ZG323, ZG324, ZG325, and ZG326—were collected, providing 75 data periods. Sensor ZG323, located near the highway, provided the primary dataset for this study, supplemented by corresponding monthly rainfall and local reservoir water levels [13]. These comprehensive data are illustrated in Figure 3, sourced from the archived records of the China Geological Environmental Monitoring Institute, Three Gorges Center. As illustrated in the figure, landslide stability is significantly influenced by rainfall and reservoir water levels. During periods of heavy rainfall, water infiltrates the soil, increasing its weight and reducing its shear strength, thereby promoting landslide activity. Similarly, fluctuations in the reservoir water levels can alter the hydrostatic pressure within the slope materials. An increase in the water level can lead to slope saturation, reducing its stability, while a decrease may lessen the support against the slope materials, potentially triggering landslides. Therefore, reservoir bank landslides induced by rainfall exhibit distinct periodic and trend characteristics.

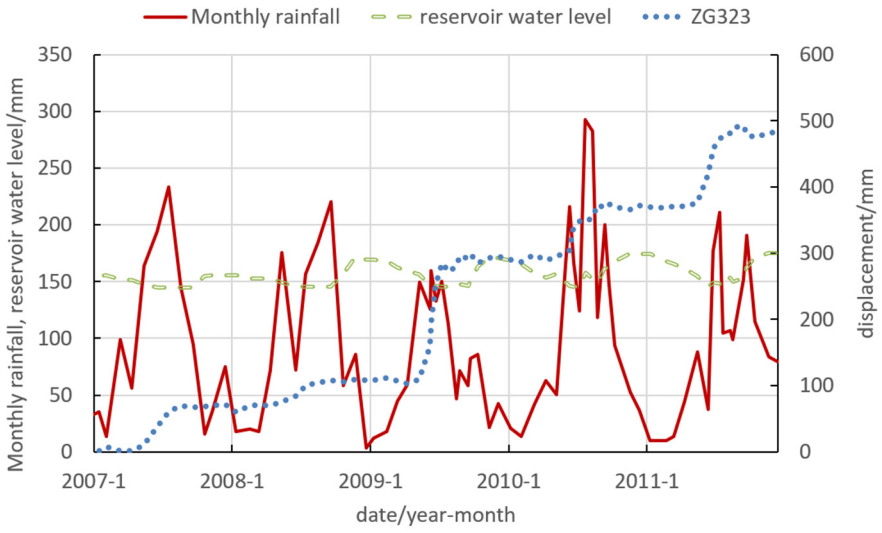

Figure 3. Monthly rainfall, reservoir levels and displacement data for the Baijiabao landslide.

Time series data form the data foundation for this study, originating from four GNSS monitoring stations distributed across the landslide body. Due to signal interruptions and equipment failures, the data from each monitoring point are not always continuous, with varying degrees of missing information. The ZG323 monitoring point has the least data missing and is conveniently located in the middle of the landslide, making it the primary dataset for this study. Missing data from ZG323 are supplemented with data from the other three stations, resulting in a continuous time series dataset spanning from January 2007 to December 2011. GNSS monitoring data are vectorial and three-dimensional, meaning their magnitude does not directly represent accurate landslide displacement. To characterize the changes more precisely in landslide displacement, we project the vectorial displacement

data along the direction of the landslide. Typically, monitoring occurs once a month, but the frequency increases during the rainy season from June to September each year, with two monitoring sessions being conducted each month. Ultimately, the number of data periods applied to the model totals 75, comprising 60 + 15 periods, where 60 represents the sum of monthly displacement data periods from January 2007 to December 2011, and 15 accounts for the sum of the second monitoring periods during the period of June to September in certain years. This ensures consistency in the direction of the data used, establishing an accurate dataset for subsequent model applications.

Given the step-like nature and evident periodicity of displacement at Baijiabao, this study proposes a landslide prediction method based on displacement decomposition using ICEEMDAN-SSA. This technique enables the precise extraction of trend and periodic terms from the landslide displacement data. A univariate LSTM model predicts the trend term, while a multivariate LSTM model addresses the periodic term. In this predictive framework, data from 2007 to 2010 serve as the training set, and data from 2011 are designated as the prediction set.

3.2. ICEEMDAN

Empirical Modal Decomposition (EMD) is a signal decomposition technique that iteratively extracts a series of intrinsic modal functions (IMFs), each representing different vibration modes at corresponding time scales. Traditional EMD algorithms often suffer from issues such as excessive mode extraction and mode aliasing. To address these issues, enhancements such as Completely Adaptive Noise Ensemble Empirical Modal Decomposition (CEEMDAN) and Improved Adaptive Noise Ensemble Empirical Modal Decomposition (ICEEMDAN) have been developed. CEEMDAN introduces adaptive noise into the original signal, followed by independent decomposition and averaging, which enhances denoising, improves accuracy, and mitigates modal aliasing to a significant extent.

ICEEMDAN, an advancement of the CEEMDAN method, is capable of decomposing complex and non-smooth signals into a trend term and a series of IMFs. In ICEEMDAN, IMFs must satisfy two conditions: (1) the number of orthogonal extreme points in any IMF must be equal or differ by no more than one throughout the signal time domain, and (2) the local mean of the function must be zero at any given moment. Through step-by-step decomposition into IMFs, ICEEMDAN achieves more accurate extraction of the signal structure, enhancing the precision and stability of signal processing analysis. ICEEMDAN is extensively applied in medical signal measurement, signal processing, image processing, and time series data analysis, offering robust methods for both analysis and processing [14].

3.3. SSA

SSA is a technique for processing nonlinear time series data. It can effectively decompose the total displacement time series into multiple sub-sequences and aggregate them into trend terms and periodic terms while removing noise. Its specific process mainly consists of four parts: embedding, decomposition, grouping, and reconstruction [15]. It is carried out through the following steps:

(1) The Creation of a Trajectory Matrix (embed step). SSA focuses on the analysis of one-dimensional and finite sequences $[x_1, x_2, \ldots, x_N]$, where N represents the length of the sequence. First, the matching window length, L, is selected and the raw time series is hysterically processed to construct the trajectory matrix, D. In most cases, the L value chosen is less than $N/2$, where N is the length of the sequence. K is defined as $N - L + 1$, and the resulting trajectory matrix, X, is a matrix of L rows and K columns.

$$X = \begin{bmatrix} x_1 & x_2 & \cdots & x_K \\ x_2 & x_3 & \cdots & x_{K+1} \\ \vdots & \vdots & \ddots & \vdots \\ x_L & x_{L+1} & \cdots & x_N \end{bmatrix} \quad (1)$$

(2) Singular Value Decomposition (SVD). The decomposition, X, is of the form $X = U\sum V^T$, where V is called the right matrix, U is called the left matrix, and non-zero values occurring only on the main diagonal are the singular values, and the rest of the elements have a value of 0. In addition, both U and V are unit orthogonal matrices, satisfying $UU^T = I, VV^T = I$. It is impractical to decompose the trajectory matrix directly, so it is first necessary to calculate the covariance matrix S of the trajectory matrix, which can be obtained by the formula $S = XX^T$. Then, the eigenvalue decomposition of the covariance matrix S is carried out to obtain a series of eigenvalues $\lambda_1 > \lambda_2 > \cdots > \lambda_L \geq 0$ and corresponding eigenvectors $U_1, U_2, \ldots, U_L$. In this step, $U = [U_1, U_2, \ldots, U_L]$, and $\sqrt{\lambda_1} > \sqrt{\lambda_2} > \cdots > \sqrt{\lambda_L} \geq 0$ for the singular spectrum of the original sequence. In addition, the trajectory matrix X may be expressed by the following formula: $X = \sum_{m=1}^{L} \sqrt{\lambda_m} U_m V_m^T, V_m = X^T U_m / \sqrt{\lambda_m}, m = 1, 2, \cdots L$. Here, the eigenvector U_i corresponding to each λ_i is called the time-empirical orthogonal function, which reveals patterns of change in time series data.

(3) Grouping. The grouping step involves dividing the set of fundamental matrices into $\{1, 2, \ldots, d\}$ cut into m disjoint subsets, $I_1, I_2, \ldots, I_m$. The singular value decomposition of X can be expressed as a combination of $X_I = X_{I_1} + \cdots + X_{I_m}$.

(4) Singular Entropy Calculation. The singular entropy is then calculated using the Shannon entropy formula applied to the normalized singular values:

$$H = -\sum_{i=1}^{r} p_i \, log(p_i) \tag{2}$$

where p_i is the normalized singular value, and r is the rank of the trajectory matrix.

(5) Reconstruction (diagonal averaging). First, the hysteresis sequence X_i is calculated in U_m projection: $a_i^m = X_i U_m = \sum_{j=1}^{L} x_{i+j} U_{m,j}, 0 \leqslant i \leqslant N - L$. Considering X_i, the ith column of the trajectory matrix X is associated with the time evolution type, and a_i^m represents the weight of X_i in the original sequence: $X_{i+1}, X_{i+2}, \cdots, X_{i+L}$. These weights are also called time principal components (TPCs). In short, the matrix consists of a_i^m, which is actually the right matrix without normalization, which is $\sqrt{\lambda_m} V_m$. Then, reconstruction is performed by using the orthogonal function of time experience and the principal component of time [16], as shown in Formula (2).

$$x_i^k = \begin{cases} \dfrac{1}{i} \displaystyle\sum_{j=1}^{i} a_{i-j}^k U_{k,j}, 1 \leq i \leq L-1 \\ \dfrac{1}{L} \displaystyle\sum_{j=1}^{L} a_{i-j}^k U_{k,j}, L \leq i \leq N-L+1 \\ \dfrac{1}{N-i+1} \displaystyle\sum_{j=i-N+L}^{i} a_{i-j}^k U_{k,j}, N-L+2 \leq i \leq N \end{cases} \tag{3}$$

In this way, the sum of all reconstructed sequences is equal to the original sequence, i.e., $x_i = \sum_{k=1}^{L} x_i^k, i = 1, 2 \ldots, N$.

3.4. LSTM

In 1997, Hochreiter and Schmidhuber first proposed the LSTM model. LSTM is a special kind of RNN, which is carefully designed. The original RNN training process, due to the extended training time and the increase in the number of network layers, is likely to have problems such as gradient bursting and gradient vanishing, which make it difficult to efficiently process very long data processing. To address this problem, LSTM adds the RNN-based memory feature, which can maintain the long-term memory of the neural network [17]. The LSTM model structure is shown in Figure 4.

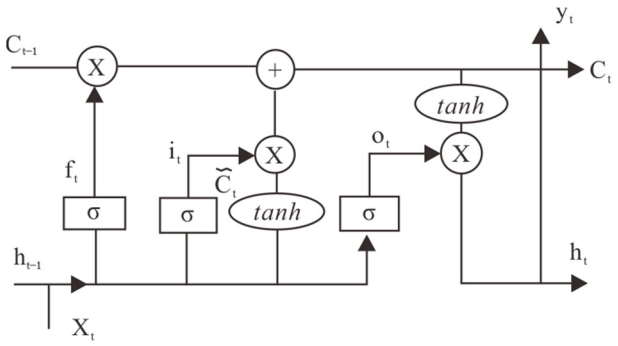

Figure 4. LSTM model structure diagram.

LSTM neurons possess three control gates, the forgetting gate (f_t), the input gate (i_t), and the output gate (o_t), with subscripts denoting moments.

Forgetting gate (f_t): Taking x_t and h_{t-1} as inputs, a value between 0 and 1 is output, which is used to determine how much to retain the cellular state C_{t-1} of the previous step, where 1 means completely retained and 0 means completely discarded. The details are shown in Formula (3) [18].

$$f_t = \sigma(W_f x_t + U_f h_{t-1}) \tag{4}$$

Input gate (i_t): First, the input gate of the sigmoid function is utilized to filter out the information that needs to be updated immediately. Then, a vector is generated at the tanh layer that determines how much information from the network input X_t at the current time step can be saved to the current cell state C_t. Finally, these two parts are combined to update the information in the current cell state C_t [19]. The details are shown in Formulas (4)–(6).

$$i_t = \sigma(W_i x_t + U_i h_{t-1}) \tag{5}$$

$$\widetilde{c}_t = tanh(W_c x_t + U_c h_{t-1}) \tag{6}$$

$$C_t = f_t * c_{t-1} + i_t * \widetilde{c}_t \tag{7}$$

Output gate (o_t): First, the sigmoid layer acts as an output gate determining how much information about the cell state C_t at the current moment can be retained into the current hidden state h_t. Then, the cell state is processed by the tanh layer, and the final output is the result of multiplying these two parts [20]. The details are shown in Formulas (7) and (8).

$$o_t = \sigma(W_o x_t + U_o h_{t-1}) \tag{8}$$

$$y_t = h_t = o_t \times tanh(c_t) \tag{9}$$

3.5. Error Analysis Index

In this paper, the root mean square error (RMSE), mean absolute error (MAE), and R^2 are used to assess the error in the prediction results.

The RMSE is the ratio of the square root of the sum of the squares of the deviations of the predicted values from the true values to the sample size, as shown in Equation (9).

The MAE is the average of the absolute errors between the predicted and observed values, as shown in Equation (10).

R^2 is calculated as $R^2 = 1 - (SSE/SST)$, where SSE is the residual sum of squares and SST is the total sum of squares. If the model is well fitted, then the SSE will be small and the R^2 value will be close to 1. If the model is poorly fitted, then the SSE will be large and the R^2 value will be close to zero.

$$\text{RMSE} = \sqrt{\frac{\sum(x - x_i)^2}{n}} \tag{10}$$

$$\mathrm{MAE} = \frac{1}{n}\sum_{i=1}^{n}|x - x_i| \tag{11}$$

where x and x_i are the true and predicted values, respectively, and n is the number of samples.

4. Results

4.1. Cumulative Displacement Decomposition

Numerous factors influence cumulative displacement, many of which exhibit cyclical patterns corresponding to seasonal weather changes. Therefore, by segregating the cyclic and trend components of the cumulative displacement, each can be predicted more effectively in isolation. This approach enhances the accuracy of cumulative displacement predictions by aligning the forecast models with the distinct behaviors exhibited by each component over time.

4.1.1. ICEEMDAN

The ICEEMDAN method is capable of decomposing data into multiple Intrinsic Mode Functions (IMFs) and a trend term. In this section, the ICEEMDAN method is employed to decompose the landslide displacement data recorded at sensor ZG323 into IMF1, IMF2, IMF3, and a trend term, as depicted in Figure 5. The sum of the IMFs, excluding the trend term, constitutes the periodic term displacement. Typically, the ICEEMDAN method extracts four to six components. As illustrated in Figure 5, the first component represents the trend term, which exhibits a distinct trend. IMF1, IMF2, and IMF3 present as progressively smoother curves, with IMF3 displaying clear periodicity. After experimental evaluation, a configuration yielding four sub-signals was selected for its enhanced accuracy in decomposing landslide displacement into trend and periodic terms.

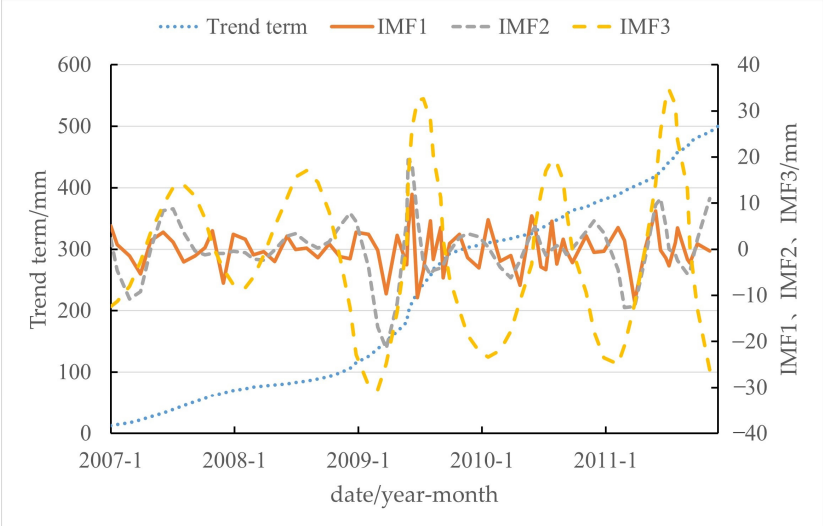

Figure 5. ICEEMDAN of cumulative displacement results.

4.1.2. SSA Decomposition

The core step of singular spectrum analysis (SSA) involves decomposing a time series into subsequences and subsequently reconstructing them. Traditionally, SSA selects the first five subsequences or customizes the number of subsequences, which can yield inaccurate results, potentially discarding crucial subsequences or reconstructing noisy ones. In this study, we employ the singular entropy method to evaluate the significance of subsequences after decomposition. The cumulative displacement is initially decomposed into L subsequences using SSA, with L set at 20. Post-decomposition, the singular entropy is calculated for each component to determine their significance, as illustrated in Figure 6a. This analysis reveals that the entropy value increment stabilizes after the tenth component, indicating

that the first ten subsequences are significant and suitable for reconstruction, while the last ten are deemed random and are discarded. The first subsequence is reconstructed as the trend term, and subsequences two through ten are reconstructed as periodic terms. The detailed results of this decomposition and reconstruction process are displayed in Figure 6b, demonstrating the efficacy of using singular entropy to enhance the accuracy of SSA decompositions.

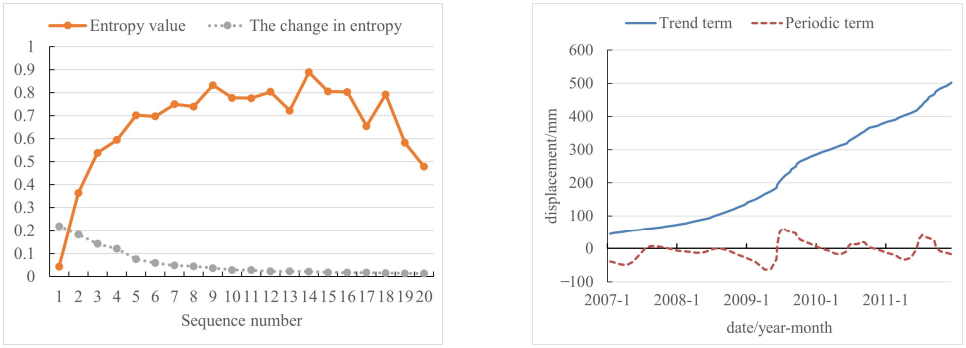

(**a**) (**b**)

Figure 6. SSA decomposes cumulative displacement. (**a**) Entropy and change in entropy. (**b**) Decomposition cumulative displacement.

4.1.3. ICEEMDAN-SSA Decomposition

The ICEEMDAN method is effective for decomposition, while the SSA method excels in denoising and reconstruction. This study proposes the combined use of these methods for joint decomposition. Initially, the ICEEMDAN method decomposes the landslide displacement data into trend and periodic terms. Subsequently, the SSA method is applied to denoise these components separately.

In this analysis, the singular entropy method is introduced to assess the significance of subsequences derived from SSA decomposition. The SSA method decomposes the trend term into L subsequences, with L set at 20. Following decomposition, the singular entropy is calculated for each component, as depicted in Figure 7a. It is observed that the entropy value increment stabilizes after the seventh component, indicating that the first seven subsequences are significant and retained as denoised trend terms, while the last thirteen subsequences, being less significant, are discarded.

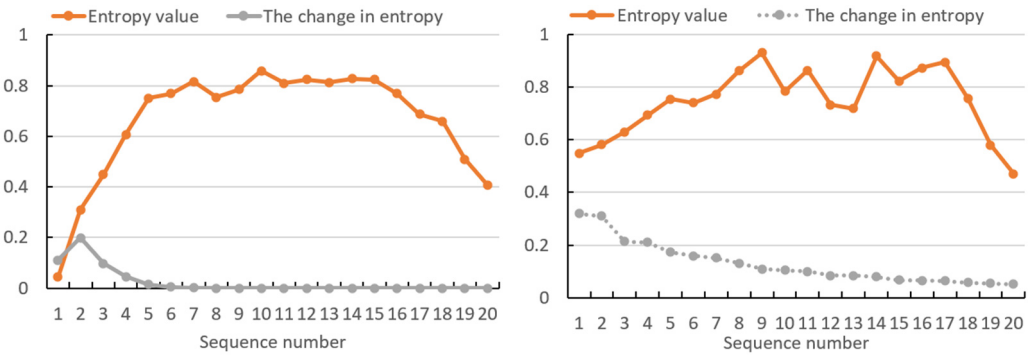

(**a**) (**b**)

Figure 7. Entropy maps for ICEEMDAN-SSA. (**a**) Entropy value and entropy change in trend term. (**b**) Entropy value and entropy change in periodic term.

Similarly, the periodic term is decomposed into subsequences, and the entropy values are calculated for each. As shown in Figure 7b, the entropy increment stabilizes after the seventeenth component. Thus, the first seventeen subsequences are considered signif-

icant and reconstructed as the periodic term after denoising, with the remaining three subsequences being discarded as noise. The reconstructed data are illustrated in Figure 8.

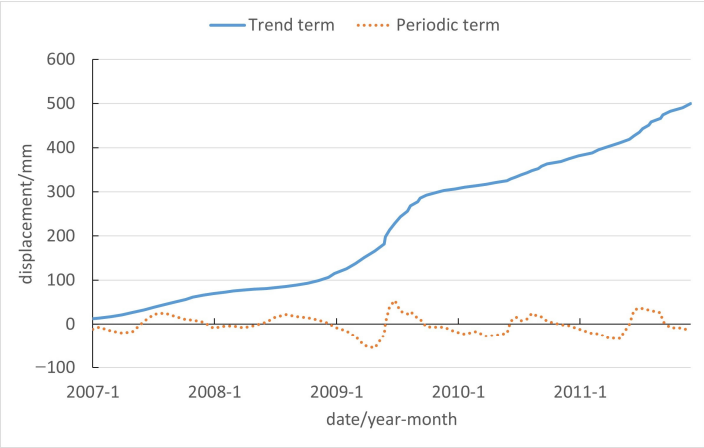

Figure 8. Plot of ICEEMDAN-SSA cumulative displacement results.

4.2. Trend Term Displacement Predictions

4.2.1. ICEEMDAN-LSTM Trend Term Prediction

LSTM models are particularly effective for issues strongly correlated with time series data, such as the prediction of landslide trend term displacements. In this study, a univariate LSTM model was utilized to predict these trend term displacements [21]. Optimal parameters were identified through automatic hyperparameter tuning using grid search; specifically, the model achieved the lowest prediction error with an input sequence length of 5 and 53 training cycles, resulting in an RMSE of 2.682 mm and an MAE of 2.157 mm. The fitting results displayed in Figure 9 illustrate that as the number of training samples increases, the predicted and actual data curves converge significantly. This convergence reduces the error progressively, especially in the prediction phase post-January 2011, where the curves overlap closely and the error approaches zero.

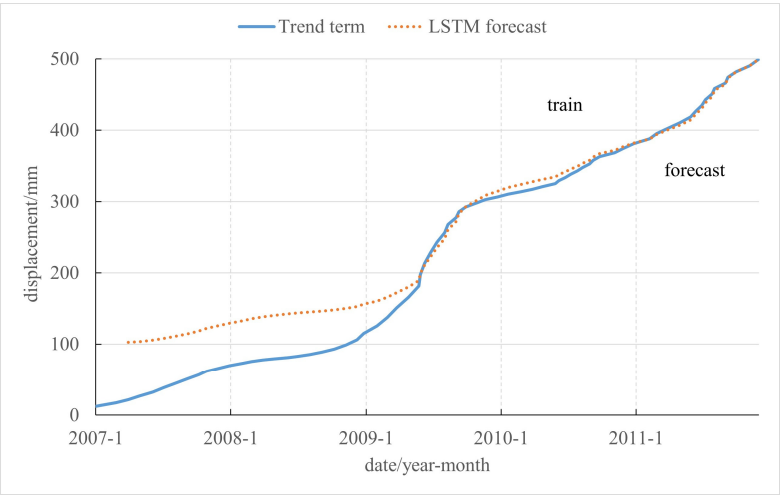

Figure 9. Plot of ICEEMDAN-LSTM trend term prediction results.

4.2.2. SSA-LSTM Trend Term Prediction

In this analysis, a univariate LSTM model was employed to fit the trend term displacements decomposed via SSA. Optimal model parameters were determined through automatic hyperparameter tuning using grid search, specifying an input sequence length

of 5 and 52 training cycles. This configuration resulted in the smallest prediction error, with an RMSE of 2.182 mm and an MAE of 1.751 mm. The model fitting results, illustrated in Figure 10, show that as the number of training samples increases, the predicted and actual data curves converge significantly, thereby reducing the prediction error. Notably, in the prediction phase—post-January 2011—the two curves overlap closely, and the error approaches zero.

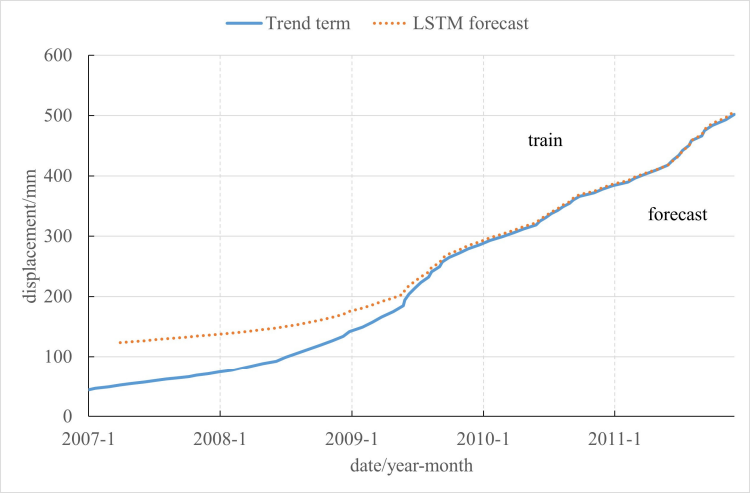

Figure 10. SSA-LSTM trend term prediction result plot.

4.2.3. ICEEMDAN-SSA-LSTM Trend Term Prediction

In this section, an LSTM model is used to predict the trend term displacements from the joint ICEEMDAN-SSA decomposition. Through automatic hyperparameter tuning using grid search, it was determined that an input sequence length of 5 and 53 training rounds resulted in the smallest prediction error, with an RMSE of 2.677 mm and an MAE of 2.152 mm. The model fitting prediction results are shown in Figure 11. As the number of training samples increases, the two curves converge, and the error decreases. In the prediction part, which includes data after January 2011, the model's predictions closely match the actual values, with the error approaching zero. Some of the hyperparameters of this LSTM model are presented in Table 1.

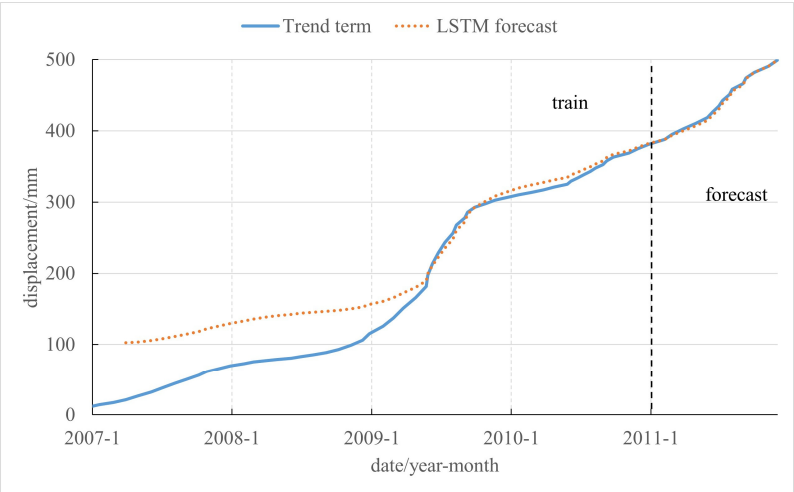

Figure 11. Plot of ICEEMDAN-SSA-LSTM trend term prediction results.

Table 1. Hyperparameters of LSTM model in trend term displacement prediction.

Hyperparameters	ICEEMDAN-SSA-LSTM
epochs	53
number of hidden layer units	50
activation function	relu
batch size	64
optimizer	Adam

4.2.4. Analysis of Results of Trend Term Projections

The trend term prediction errors of the three methods—ICEEMDAN-LSTM, SSA-LSTM, and ICEEMDAN-SSA-LSTM—are shown in Table 2. The prediction errors for the trend term across these models are not large, with a relative error of less than 0.01 and an R^2 value higher than 0.99, indicating an accuracy of 99% and very precise trend term predictions over time. The primary reason for this high accuracy is that the LSTM model not only addresses the vanishing gradient problem but also fully captures the patterns in historical trend term data. This demonstrates that the LSTM model has significant advantages in predicting time series data, making it highly suitable for landslide prediction.

Table 2. Table of forecast errors for trend terms.

Model	RMSE/mm	MAE/mm	Relative Error/%	R^2/%
ICEEMDAN-LSTM	2.682	2.157	0.5	99.97
SSA-LSTM	2.182	1.751	0.6	99.83
ICEEMDAN-SSA-LSTM	2.677	2.152	0.5	99.97

4.3. Periodic Term Displacement Predictions

4.3.1. Multivariate LSTM Feature Factor Selection

In this study, the correlation between two continuous variables was assessed using Pearson correlation analysis. Pearson correlation coefficients range from −1 to 1, where −1 indicates a negative correlation, 1 indicates a positive correlation, and 0 indicates no correlation. The closer the value of the correlation coefficient is to zero, the weaker the correlation between the variables; conversely, the closer the value is to −1 or 1, the stronger the correlation. Generally, a coefficient less than 0.2 indicates no correlation, between 0.2 and 0.5 indicates a weak correlation, and greater than 0.5 indicates a strong correlation, as shown in Formula (11):

$$r = \frac{\sum XY - \frac{\sum X \sum Y}{N}}{\sqrt{\left(\sum X^2 - \frac{(\sum X)^2}{N}\right)\left(\sum Y^2 - \frac{(\sum Y)^2}{N}\right)}} \quad (12)$$

Most landslide deformations are caused by rainfall and changes in reservoir water levels. As the water level rises, it deforms the landslide, creating numerous cracks in the ground surface, which facilitates the storage and transfer of surface water within the landslide. This process significantly increases the impact of rainfall, particularly heavy rainfall, on landslide activity. Using data from the Baijiabao landslide from November 2006 to December 2011, a Pearson correlation analysis was conducted to examine the relationships between displacement, rainfall, and the reservoir level. As shown in Table 3, the Pearson correlation coefficients for the displacement increment in the first two months, displacement increment in the first three months, rainfall in the current and previous month, and rainfall in the first two months are all greater than 0.5. This indicates a strong correlation between these factors and the periodic term of displacement. Therefore, these five terms are used as valid characterization factors [22].

Table 3. Impact factors' Pearson calculations.

	Characteristic Factor	Pearson Correlation
displacement	Cumulative displacement	0.217
	Displacement increment for the month	0.312
	Displacement increments in the first two months	0.501
	Displacement increments in the first three months	0.638
quantity of rainfall	Rainfall for the month	0.395
	Rainfall for two months	0.528
	Rainfall in the previous month	0.552
	Rainfall in the first two months	0.646
reservoir level	Reservoir level for the month	−0.432
	Amount of change in reservoir level during the month	0.321
	Amount of change in reservoir level in two months	0.273

4.3.2. ICEEMDAN-LSTM Periodic Term Prediction

The multivariate LSTM model not only considers the overall effect of historical displacement data but also incorporates data from other effective characterization factors when making predictions. This approach improves the accuracy of the variable weights corresponding to the displacements and enhances the performance of the predictions. Therefore, this study employs a multivariate LSTM model, incorporating data such as the displacement increment from the first two months, displacement increment from the first three months, rainfall from the current and previous month, and rainfall from the first two months, all with Pearson correlation coefficients greater than 0.5 [23].

To optimize the use of the multivariate LSTM model, the data were divided into training and prediction sets in a 4:1 ratio. The training set was iteratively trained to obtain suitable network parameters, and the model's performance was evaluated using the prediction set. Through automatic hyperparameter tuning using grid search, it was determined that the optimal input sequence length was 6 and the number of training rounds was 500, resulting in the smallest prediction error, with an RMSE of 4.762 mm and an MAE of 3.833 mm. The model fitting prediction results are illustrated in Figure 12.

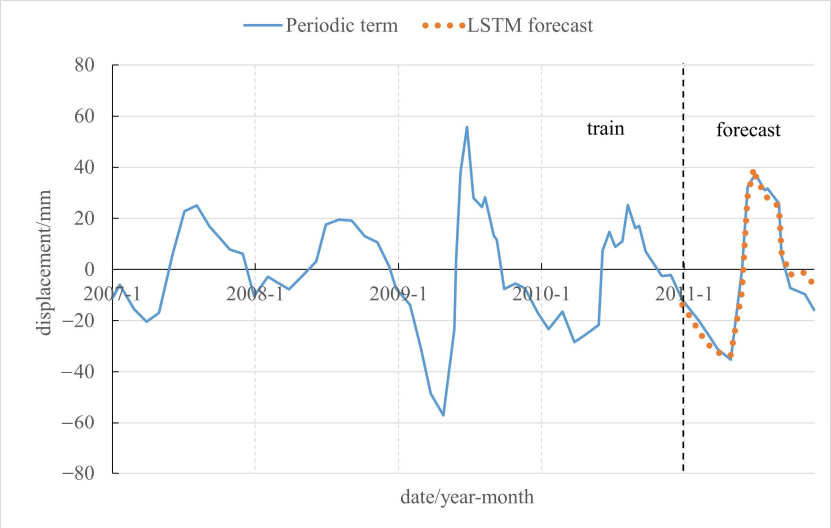

Figure 12. Plot of ICEEMDAN-LSTM cycle term prediction results.

4.3.3. SSA-LSTM Periodic Term Prediction

In this section, a multivariate LSTM model is used to predict the periodic terms, incorporating the data with Pearson correlation coefficients greater than 0.5. The data were divided into training and prediction sets in a ratio of 4:1. The training set was iteratively

trained to obtain suitable network parameters, and the model's performance was evaluated using the prediction set. Through automatic hyperparameter tuning using grid search, it was determined that the optimal input sequence length was 5 and the number of training rounds was 600, resulting in the smallest prediction error, with an RMSE of 6.472 mm and an MAE of 4.992 mm. The model fitting prediction results are illustrated in Figure 13.

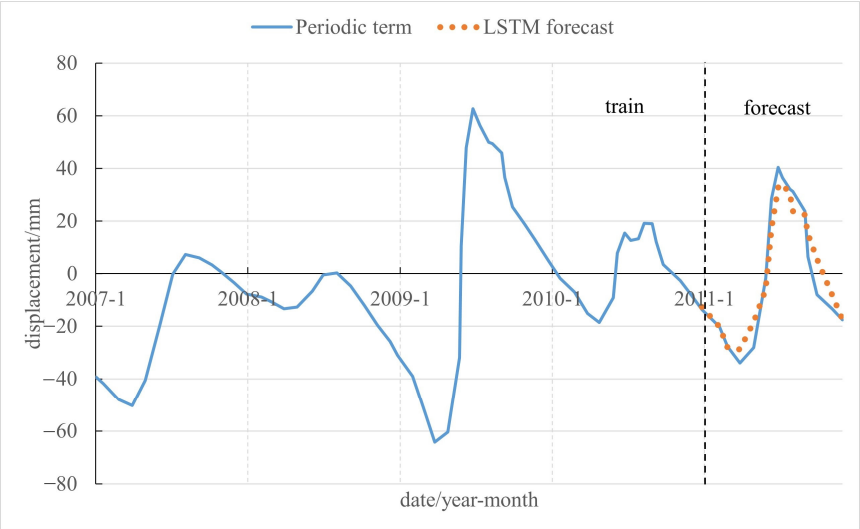

Figure 13. SSA-LSTM cycle term prediction result plot.

4.3.4. ICEEMDAN-SSA-LSTM Periodic Term Prediction

In this section, a multivariate LSTM model is employed to predict the periodic terms, incorporating data with Pearson correlation coefficients greater than 0.5. The data were divided into training and prediction sets in a ratio of 4:1. The training set was iteratively trained to obtain suitable network parameters, and the model's performance was evaluated using the prediction set. Through automatic hyperparameter tuning using grid search, it was determined that the optimal input sequence length was 6 and the number of training rounds was 470, resulting in the smallest prediction error with an RMSE of 4.366 mm and an MAE of 3.806 mm. The model fitting prediction results are illustrated in Figure 14, showing that the LSTM predictions closely match the actual results, indicating good predictive performance. Some of the hyperparameters of this LSTM model are presented in Table 4.

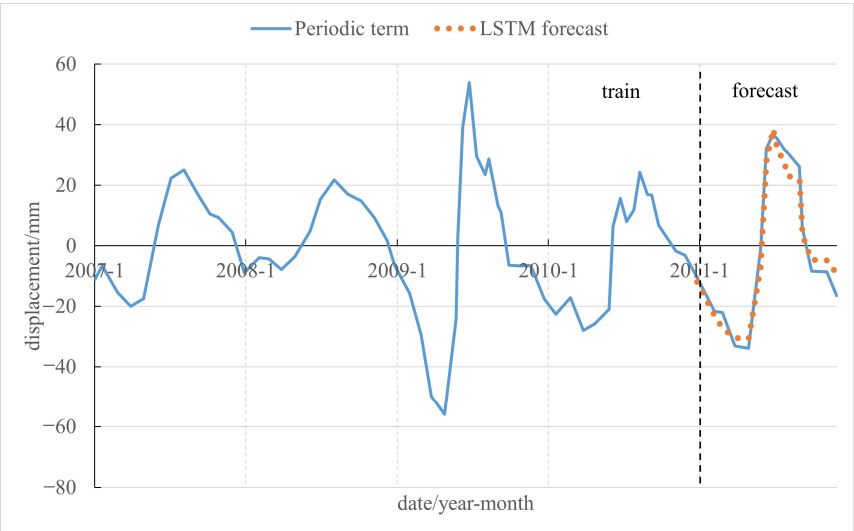

Figure 14. ICEEMDAN-SSA-LSTM cycle term prediction result map.

Table 4. Hyperparameters of LSTM model in periodic term displacement prediction.

Hyperparameters	ICEEMDAN-SSA-LSTM
epochs	470
number of hidden layer units	50
activation function	tanh
batch size	10
optimizer	Adam

4.3.5. An Analysis of the Results of the Cyclical Projections

In the prediction model, data from 2007 to 2010 are used as the training set, while data from 2011 are used as the prediction set. The specific displacement values for 2011 predicted by the periodic terms of each method are shown in Table 5. The cycle term prediction results of the three methods—ICEEMDAN-LSTM, SSA-LSTM, and ICEEMDAN-SSA-LSTM—are depicted in Figure 15, with the corresponding errors listed in Table 6. Among these models, the ICEEMDAN-SSA-LSTM model yields the best prediction performance, with an RMSE of 4.366 mm and an MAE of 3.806 mm. These values are lower than the RMSE and MAE of the ICEEMDAN-LSTM model (4.762 mm and 3.833 mm, respectively) and the SSA-LSTM model (6.472 mm and 4.992 mm, respectively). Additionally, the R^2 value of the ICEEMDAN-SSA-LSTM model is 97.5%, which is higher than the value of 96.3% of the ICEEMDAN-LSTM model and the value of 92.8% of the SSA-LSTM model [24].

Table 5. The specific values of the periodic term prediction for the five methods.

Date	Periodic Term/mm	ICEEMDAN-LSTM/mm	SSA-LSTM/mm	ICEEMDAN-SSA-LSTM/mm	ICEEMDAN-SSA-RNN/mm	ICEEMDAN-SSA-SVM/mm
January 2011	−11.852	−13.769	−12.584	−11.999	3.120	−9.514
February 2011	−19.962	−23.744	−20.220	−23.061	−7.082	−11.816
March 2011	−24.160	−28.647	−27.899	−27.211	−13.323	−17.296
April 2011	−31.197	−32.549	−28.817	−30.432	−12.273	−21.824
May 2011	−35.284	−33.642	−18.472	−30.714	−10.422	−27.672
June 2011	0.065	−8.780	−6.120	−7.208	3.693	−30.850
June 2011	32.100	28.183	17.633	28.198	24.615	−16.935
July 2011	36.336	39.592	32.986	38.590	38.167	17.265
July 2011	35.869	33.359	34.191	32.294	36.932	39.823
August 2011	31.061	30.878	30.089	27.140	36.569	32.661
August 2011	31.620	27.691	23.798	23.162	33.503	17.783
September 2011	25.787	24.698	22.390	21.782	30.642	15.408
September 2011	5.400	6.434	15.254	3.458	29.707	17.692
October 2011	−7.295	−1.942	5.707	−4.605	28.662	6.949
November 2011	−9.685	−1.248	−8.176	−4.874	25.294	−12.627
December 2011	−15.806	−6.204	−17.208	−9.367	20.068	−19.491

Table 6. Errors in forecasting periodic terms.

	RMSE/mm	MAE/mm	R^2/%
ICEEMDAN-LSTM	4.762	3.833	96.3
SSA-LSTM	6.472	4.992	92.8
ICEEMDAN-SSA-LSTM	4.366	3.806	97.5
RNN	19.945	15.343	72.3
SVM	16.584	12.748	56.6

The RNN and SVM models were developed to predict the periodic terms, and the root mean square error (RMSE) and mean absolute error (MAE) were used for evaluation. The prediction results are shown in Figure 15, and the errors are listed in Table 6. Among the three models, the LSTM model yielded the best prediction results, with an RMSE of 4.366 mm and an MAE of 3.806 mm. These values are significantly smaller compared to the

values of 19.945 mm and 15.343 mm for the RNN model and 16.584 mm and 12.748 mm for the SVM model. Additionally, the R^2 value of the ICEEMDAN-SSA-LSTM model is 97.5%, surpassing the value of 72.3% of the RNN model and the value of 56.6% of the SVM model.

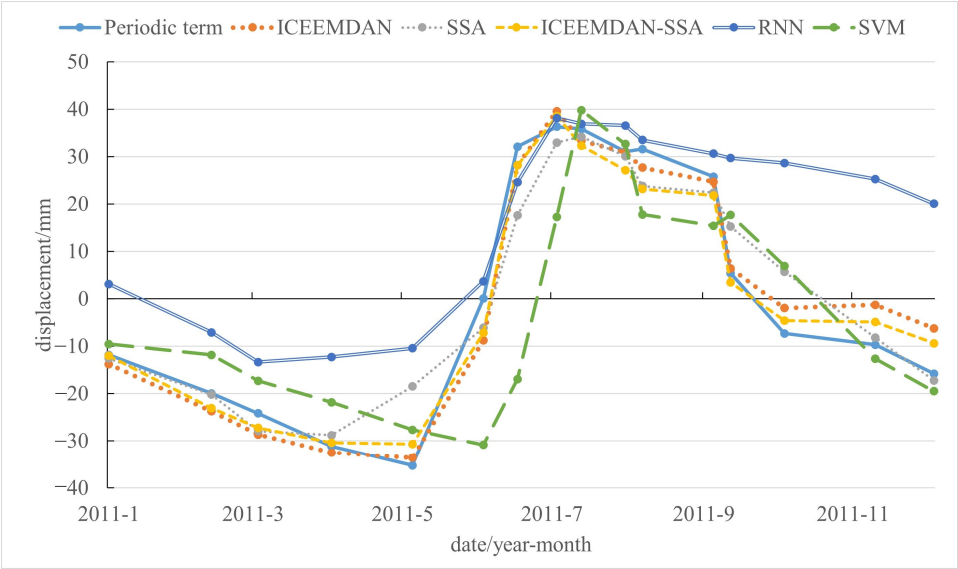

Figure 15. A comparison of the results of the cyclical term predictions.

The forecast results in Table 7 are analyzed from the perspective of forecast time. The data were divided into periods from January to June and from July to December, and the corresponding errors were calculated. The error results are shown in Table 5. It is evident that the error of the ICEEMDAN-SSA-LSTM model from January to June is significantly smaller than that of the other models, demonstrating the feasibility of this model for displacement prediction. The error of the ICEEMDAN-SSA-LSTM model from July to December is generally smaller than that of the other models. Only the MAE of the ICEEMDAN-SSA-LSTM model from July to December is slightly larger than that of the ICEEMDAN-LSTM model. When analyzing the error for the entire year of 2011, from January to June and from July to December, the ICEEMDAN-SSA-LSTM model consistently outperforms the ICEEMDAN-LSTM model and significantly outperforms the other models.

Table 7. Segmentation errors in model predictions.

	January–June RMSE/mm	January–June MAE/mm	July–December RMSE/mm	July–December MAE/mm
ICEEMDAN-LSTM	4.411	3.706	5.019	3.933
SSA-LSTM	8.868	6.368	6.307	4.776
ICEEMDAN-SSA-LSTM	3.937	3.258	4.672	4.231
RNN	14.893	13.368	22.251	16.251
SVM	22.756	16.326	10.839	9.111

To more accurately determine the superiority of the ICEEMDAN-SSA-LSTM model over the ICEEMDAN-LSTM model, three separate experiments were conducted using these two models. The resultant errors and average errors are shown in Table 8. It can be observed that the average RMSE and average MAE of the ICEEMDAN-SSA-LSTM model are smaller than those of the ICEEMDAN-LSTM model. The average R^2 of the ICEEMDAN-SSA-LSTM model is 97.8%, which is larger than the value of 96.9% of the ICEEMDAN-LSTM model. Therefore, the ICEEMDAN-SSA-LSTM model is superior to the ICEEMDAN-LSTM model.

Table 8. Three experimental error results.

	ICEEMDAN-LSTM	ICEEMDAN-SSA-LSTM
First RMSE/mm	4.762	4.366
First MAE/mm	3.833	3.806
First R^2/%	96.3	97.5
Second RMSE/mm	6.620	5.675
Second MAE/mm	5.300	5.040
Second R^2/%	96.8	97.4
Third RMSE/mm	5.602	5.001
Third MAE/mm	4.518	3.289
Third R^2/%	97.5	98.4
Average RMSE/mm	5.661	5.014
Average MAE/mm	4.550	4.052
Average R^2/%	96.9	97.8

Among all of the prediction models, the RNN model exhibits the largest discrepancy from the original data and the highest prediction error. This is primarily due to the inherent limitation of the RNN model, specifically the vanishing gradient problem, which restricts its memory to short-term sequences and renders it unsuitable for long-sequence data like landslide displacement. The SVM model also demonstrates suboptimal prediction performance, mainly because it cannot effectively utilize historical data and only learns from current data points. In contrast, the LSTM model achieves the best prediction performance. The LSTM model not only addresses the vanishing gradient problem but also fully exploits the historical displacement data, uncovering the connections between displacement data, historical monthly rainfall, and reservoir levels [25]. This demonstrates that the LSTM model exhibits significant advantages in data mining when incorporating influencing factors, thereby proving the appropriateness of the multivariate LSTM model for landslide displacement prediction [26].

4.4. Cumulative Displacement Prediction

After decomposing the displacement data using the ICEEMDAN-SSA model, the trend term predicted by the univariate LSTM and the periodic term predicted by the multivariate LSTM are summed to obtain the cumulative displacement, as illustrated in Figure 16. The average relative error is calculated to be 0.011, demonstrating the effectiveness of the ICEEMDAN-SSA decomposition and the LSTM model's ability to accurately predict landslide displacement changes. In this study, the univariate LSTM model predicts the trend term displacement, which remains largely unaffected by other influences, while the multivariate LSTM model predicts the periodic term displacement, which is influenced by factors such as rainfall and reservoir levels. This combined approach enhances the prediction accuracy of the model.

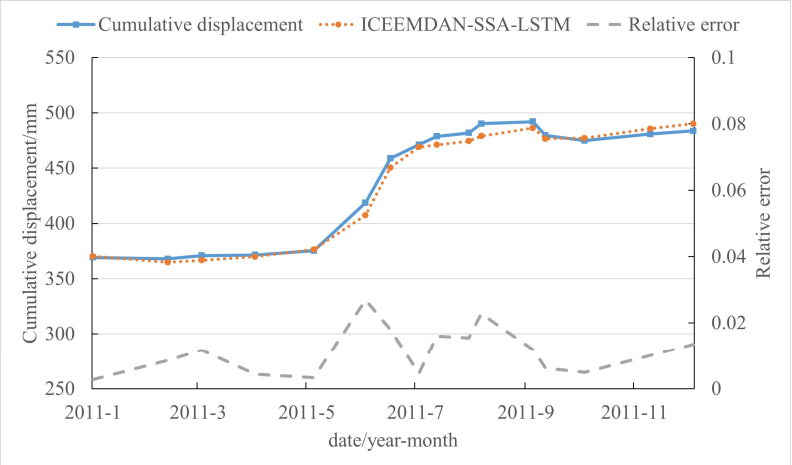

Figure 16. Comparison of cumulative displacement predictions.

5. Summary and Outlook

5.1. Conclusions

This paper proposes the ICEEMDAN-SSA-LSTM model for predicting landslide displacement data. Firstly, the landslide displacement time series is decomposed into trend and periodic terms using the ICEEMDAN method. Subsequently, the trend and periodic terms are processed by singular entropy-improved singular spectrum analysis (SSA) to obtain the denoised trend and periodic terms. These terms are then predicted using the LSTM model, resulting in an optimized landslide displacement model. This model demonstrates higher accuracy compared to models using SSA or ICEEMDAN alone. The joint decomposition of displacement by ICEEMDAN and SSA is more accurate than that using ICEEMDAN alone. Furthermore, integrating the LSTM model with the joint ICEEMDAN and SSA decomposition yields the best prediction results among the three types of models, aligning more closely with the actual evolutionary characteristics.

While traditional methods typically employ a single decomposition method, this study utilizes both ICEEMDAN and SSA to decompose landslide displacement data. The advantages of accurately decomposing displacements into trend and periodic components are multifaceted. Firstly, it streamlines the analytical process by facilitating a more intuitive grasp of both the overall direction and intricate variations within the data, thereby mitigating the challenges posed by intricate datasets. Secondly, it enhances forecasting effectiveness. Comprehending the trend components aids in identifying the long-term trajectory of the data, whereas recognizing periodic components fosters predictions of impending cyclical shifts, ultimately refining forecast accuracy. Lastly, it optimizes model construction, ensuring a more robust and predictive framework. Decomposition provides deeper insights into how each component affects overall displacement, enabling the construction of more accurate models. In summary, dividing displacements into trend and cyclic terms constitutes a powerful analytical method. It offers an effective means for the in-depth interpretation and efficient management of complex data across various fields.

The model developed in this study holds significant practical implications for disaster management and prediction in real-world settings. By providing accurate and timely predictions of landslide displacements, it enables authorities and stakeholders to implement preventative measures, optimize evacuation plans, and allocate resources more effectively. This proactive approach minimizes potential casualties and economic losses, ultimately enhancing the resilience of communities to landslide hazards.

5.2. Innovation Point

In this study, landslide displacement prediction modeling is approached from the perspective of displacement decomposition. The main innovations are as follows:

(1) ICEEMDAN, an improvement of the CEEMDAN method, accurately decomposes complex and non-smooth signals into a trend term and a series of Intrinsic Mode Functions (IMFs).

(2) Utilizing singular entropy and its increments allows for the easy distinction of useful information within the sequence. The singular entropy-improved SSA method effectively removes random terms from landslide displacements, extracts effective sequences, and reconstructs them into trend and periodic terms.

(3) The displacement of the Baijiabao landslide is characterized by a step-up curve. A Pearson correlation analysis with rainfall and reservoir level data indicates that these factors significantly influence the Baijiabao landslide.

(4) The multivariate LSTM model not only considers the overall role of historical displacement data when making predictions, but also integrates historical rainfall and reservoir level data. This precise adjustment of corresponding displacement weights for each variable results in improved prediction performance.

(5) The LSTM model addresses the vanishing gradient problem and fully leverages the historical displacement data's changing patterns. This makes it particularly suitable for predicting dynamically changing landslide displacement data.

5.3. Outlook

This study primarily proposes two models for landslide displacement prediction, demonstrating superior predictive accuracy for the research objectives outlined herein. These models contribute to advancing subsequent research in landslide prediction. However, the actual situation is highly complex, and the models proposed in this study represent only a small part of the broader field of landslide prediction, which still faces many challenging issues:

(1) Landslides are influenced by a multitude of factors, including geological conditions, topography, and human activities. This complexity renders landslide prediction extremely challenging. In this study, only a limited set of conditions were considered. A key unresolved issue is how to integrate all relevant variables to enhance the accuracy of landslide predictions.

(2) Time series data exhibit both temporal and spatial characteristics. This study primarily addresses the temporal characteristics of landslide displacement, integrating various time series-related models, but it does not account for spatial characteristics. Spatial characteristics involve extensive geological theories, necessitating a foundational understanding of geology. By integrating both temporal and spatial characteristics, more accurate landslide displacement predictions can be achieved, thereby effectively mitigating the impact of landslide disasters on human life and property.

In summary, the in-depth study of landslide phenomena remains in an exploratory phase. To fundamentally address landslide issues and prevent further damage to human life and property, a comprehensive approach is required. This approach should encompass theoretical analysis, real-time monitoring, and early warning systems, promoting the coordinated development of these strategies. The collective wisdom and relentless efforts of researchers are essential to advancing landslide research to new heights.

Author Contributions: Conceptualization, K.Y. and Y.W.; methodology, K.Y.; software, K.Y.; formal analysis, K.Y.; investigation, G.D.; resources, Y.W.; data curation, Y.W.; writing—original draft preparation, K.Y.; writing—review and editing, G.D.; visualization, K.Y.; supervision, G.D.; project administration, Y.W.; funding acquisition, Y.W. All authors have read and agreed to the published version of the manuscript.

Funding: This research is supported by the middle-aged and young talents project of the Hubei Provincial Department of Education (Q20191504) and the Open Fund of the Key Laboratory of Geological Hazards on the Three Gorges Reservoir China, Three Gorges University (2022KDZ05).

Data Availability Statement: The data presented in this study are available upon request from the corresponding author.

Conflicts of Interest: The authors declare no conflicts of interest.

References

1. Shihabudheen, K.V.; Pillai, G.N.; Peethambaran, B. Prediction of landslide displacement with controlling factors using extreme learning adaptive neuro-fuzzy inference system (ELANFIS). *Appl. Soft Comput.* **2017**, *61*, 892–904. [CrossRef]
2. Wang, Y.; Tang, H.; Wen, T. Direct Interval Prediction of Landslide Displacements Using Least Squares Support Vector Machines. *Complexity* **2020**, *2020*, 7082594. [CrossRef]
3. Wu, L.Z.; Li, S.H.; Huang, R.Q.; Xu, Q. A new grey prediction model and its application to predicting landslide displacement. *Appl. Soft Comput.* **2020**, *95*, 106543. [CrossRef]
4. Lin, Z.; Sun, X.; Ji, Y. Landslide Displacement Prediction Based on Time Series Analysis and Double-BiLSTM Model. *Int. J. Environ. Res. Public Health* **2022**, *19*, 2077. [CrossRef]
5. Utomo, D.; Chen, S.F.; Hsiung, P.A. Landslide prediction with model switching. *Appl. Sci.* **2019**, *9*, 1839. [CrossRef]
6. Zhu, X.; Ma, S.Q.; Xu, Q.; Liu, W.D.; Quan, Z.A.; Wang, Y.; Huang, D.; Hu, M. Landslide Displacement Prediction Combining PSO and LSSVM Model. *Water* **2023**, *15*, 612. [CrossRef]
7. Liu, Z.Q.; Guo, D.; Lacasse, S.; Li, J.H.; Yang, B.B.; Choi, J.C. Algorithms for intelligent prediction of landslide displacements. *J. Zhejiang Univ. Sci. A* **2020**, *21*, 412–429. [CrossRef]
8. Glade, T.; Yin, K. Landslide Displacement Prediction Combining LSTM and SVR Algorithms: A Case Study of Shengjibao Landslide from the Three Gorges Reservoir Area. *Appl. Sci.* **2020**, *10*, 7830. [CrossRef]

9. Wang, M.; Xu, S.C.; Yi, W. Landslide deformation prediction based on singular spectrum analysis. *Hydropower Gener.* **2018**, *44*, 28–30.
10. Nava, L.; Carraro, E.; Reyes-Carmona, C.; Puliero, S.; Bhuyan, K.; Rosi, A.; Monserrat, O.; Floris, M.; Meena, S.R.; Galve, J.P.; et al. Landslide displacement forecasting using deep learning and monitoring data across selected sites. *Landslides* **2023**, *20*, 2111–2129. [CrossRef]
11. Yang, B.B.; Yin, K.L.; Liang, X.; Zhao, H.Y. Deformation characteristics and evolutionary simulation of the Maliu Forest landslide in the Three Gorges reservoir area. *Geosci. Technol. Bull.* **2020**, *39*, 122–129.
12. Long, J.; Li, C.; Liu, Y.; Feng, P.; Zuo, Q. A multi-feature fusion transfer learning method for displacement prediction of rainfall reservoir-induced landslide with step-like deformation characteristics. *Eng. Geol.* **2022**, *297*, 106494. [CrossRef]
13. Shang, M.; Liao, F.; Ma, R.; Liu, Y.T. Quantitative analysis of the correlation between the deformation of Baijabao landslide and reservoir water level and rainfall. *J. Eng. Geol.* **2021**, *29*, 742–750. [CrossRef]
14. Zhang, Y.L.; Bian, J.W.; Ding, K.H.; Ran, J.N.; Liu, W.P. Reconstruction of GNSS coordinate time series based on improved empirical mode decomposition and SSA joint algorithm. *Geod. Geodyn.* **2022**, *42*, 904–909. [CrossRef]
15. Mukhopadhyay, S.K.; Krishnan, S. A singular spectrum analysis-based model-free electrocardiogram denoising technique. *Comput. Methods Programs Biomed.* **2020**, *188*, 105304. [CrossRef] [PubMed]
16. Kumar, P.; Sihag, P.; Sharma, A.; Pathania, A.; Singh, R.; Chaturvedi, P.; Mali, N.; Uday, K.V.; Dutt, V. Prediction of real-world slope movements via recurrent and non-recurrent neural network algorithms: A case study of the Tangni landslide. *Indian Geotech. J.* **2021**, *51*, 788–810. [CrossRef]
17. Zhang, K.; Zhang, K.; Cai, C.X.; Liu, W.L.; Xie, J.B. Displacement Prediction of step-like Landslides based on Feature Optimization and VMD-Bi-LSTM: A case study of the Bazimen and Baishuihe Landslides in the Three Gorges, China. *Bull. Eng. Geol. Environ.* **2021**, *80*, 8481–8502. [CrossRef]
18. Xing, Y.; Yue, J.P.; Chen, C. Interval Estimation of Landslide Displacement Prediction based on Time Series Decomposition and Long Short-term Memory Network. *IEEE Access* **2019**, *8*, 3187–3196. [CrossRef]
19. Niu, X.X.; Ma, J.W.; Wang, Y.K.; Zhang, J.R.; Chen, H.J.; Tang, H.M. A novel decomposition-ensemble learning model based on ensemble empirical mode decomposition and recurrent neural network for landslide displacement prediction. *Appl. Sci.* **2021**, *11*, 4684. [CrossRef]
20. Aggarwal, A.; Alshehri, M.; Kumar, M.; Alfarraj, O.; Sharma, P.; Pardasani, K.R. Landslide data analysis using various time-series forecasting models. *Comput. Electr. Eng.* **2020**, *88*, 106858. [CrossRef]
21. Xie, P.H.; Zhou, A.G.; Chai, B. The application of long short-term memory (LSTM) method on displacement prediction of multifactor-induced landslides. *IEEE Access* **2019**, *7*, 54305–54311. [CrossRef]
22. Gong, S.S.; Yang, S.Y.; She, J.K.; Li, W.Q.; Lu, S.F. Multivariate Time Series Prediction for Loss of Coolant Accidents with a Zigmoid-Based LSTM. *Front. Energy Res.* **2022**, *10*, 852349. [CrossRef]
23. Rodriguez, A.X.; Salazar, D.A. Methodology for the prediction of fluid production in the waterflooding process based on multivariate long–short term memory neural networks. *J. Pet. Sci. Eng.* **2022**, *208*, 109715. [CrossRef]
24. Kim, G.B.; Hwang, C.I.; Choi, M.R. PCA-based multivariate LSTM model for predicting natural groundwater level variations in a time-series record affected by anthropogenic factors. *Environ. Earth Sci.* **2021**, *80*, 657. [CrossRef]
25. Mandal, A.K.; Sen, R.; Goswami, S.; Chakraborty, B. Comparative study of univariate and multivariate long short-term memory for very short-term forecasting of global horizontal irradiance. *Symmetry* **2021**, *13*, 1544. [CrossRef]
26. Duan, G.H.; Su, Y.W.; Fu, J. Landslide Displacement Prediction Based on Multivariate LSTM Model. *Int. J. Environ. Res. Public Health* **2023**, *20*, 1167. [CrossRef]